

Article

Open Access



Impact of *in coin cell* atmosphere on lithium metal battery performance

Sebastian P. Kühn¹, Matthias Weiling¹, Diddo Diddens¹, Masoud Baghernejad¹, Martin Winter^{1,2}, Isidora Cekic-Laskovic^{1,*}

¹Helmholtz-Institute Münster, Forschungszentrum Jülich GmbH, Münster 48149, Germany.

²MEET Battery Research Center, University of Münster, Münster 48149, Germany.

*Correspondence to: Dr. Isidora Cekic-Laskovic, Ionics in Energy Storage (IEK-12), Helmholtz-Institute Münster, Forschungszentrum Jülich GmbH, Corrensstrasse 48, Münster 48149, Germany. E-mail: i.cekic-laskovic@fz-juelich.de

How to cite this article: Kühn SP, Weiling M, Diddens D, Baghernejad M, Winter M, Cekic-Laskovic I. Impact of *in coin cell* atmosphere on lithium metal battery performance. *Energy Mater* 2023;3:300020. <https://dx.doi.org/10.20517/energymater.2023.07>

Received: 8 Feb 2023 **First Decision:** 3 Mar 2023 **Revised:** 20 Mar 2023 **Accepted:** 28 Mar 2023 **Published:** 8 May 2023

Academic Editor: Jia-Qi Huang **Copy Editor:** Fangling Lan **Production Editor:** Fangling Lan

Abstract

Research on lithium metal as a high-capacity anode for future lithium metal batteries (LMBs) is currently at an all-time high. To date, the different influences of a highly pure argon glovebox (GB) and an industry-relevant ambient dry room (DR) atmosphere have received little attention in the scientific community. In this paper, we report on the impact of *in coin cell* atmosphere (ICCA) on the performance of an LMB as well as its interphase characteristics and properties in combination with three organic carbonate-based electrolytes with and without two well-known interphase-forming additives, namely fluoroethylene carbonate (FEC) and vinylene carbonate (VC). The results obtained from this carefully executed systematic study show a substantial impact of the ICCA on solid electrolyte interphase (SEI) resistance (R_{SEI}) and lithium stripping/plating homogeneity. In a transition metal cathode (NMC811) containing LMBs, a DR ICCA results in an up to 50% increase in lifetime due to the improved chemical composition of the cathode electrolyte interphase (CEI). Furthermore, different impacts on electrode characteristics and cell performance were observed depending on the utilized functional additive. Since this study focuses on a largely overlooked influential factor of LMB performance, it highlights the importance of comparability and transparency in published research and the importance of taking differences between research and industrial environments into consideration in the aim of establishing and commercializing LMB cell components.



© The Author(s) 2023. **Open Access** This article is licensed under a Creative Commons Attribution 4.0 International License (<https://creativecommons.org/licenses/by/4.0/>), which permits unrestricted use, sharing, adaptation, distribution and reproduction in any medium or format, for any purpose, even commercially, as long as you give appropriate credit to the original author(s) and the source, provide a link to the Creative Commons license, and indicate if changes were made.



Keywords: Lithium metal battery, *in coin cell* atmosphere, liquid electrolyte, film-forming additive, solid electrolyte interphase, cathode electrolyte interphase

INTRODUCTION

The application of lithium metal as the “holy grail”^[1-3] electrode material has been a topic in academia and industry for more than 40 years. The high theoretical specific capacity ($3,860 \text{ mAh g}^{-1}$)^[4,5] and the low standard reduction potential (-3.04 V vs. SHE) make lithium metal an ideal material for future high energy density batteries. To date, the main challenge for commercial liquid electrolyte-based LMBs to overcome is inhomogeneous stripping/plating coinciding with the formation of high surface area lithium (HSAL), also known as dendritic morphology^[6]. There have been a variety of approaches to stabilize the lithium metal anode, the solid electrolyte interphase (SEI)^[7-9], and improve lithium stripping/plating behavior. These include stabilizing functional electrolyte additives^[2,10-12], lithium metal pre-treatment and artificial SEIs^[13-17], lithium metal host materials^[18-20], and the application of external pressure^[21,22]. Multiple publications have also suggested guidelines and benchmarks for battery performance characterization to enhance research comparability^[23-27]. Another external factor that can influence the performance of battery electrodes is the storage atmosphere. In particular, the degradation of cathode materials in an ambient atmosphere has been the subject of numerous publications^[28,29]. However, the reactivity of lithium metal with its surrounding atmosphere, resulting in different compositions of the native passivation layer covering the lithium surface, has only recently come into focus^[7,30,31]. Furthermore, the influence of different storage atmospheres on lithium metal electrode performance has - to the best of our knowledge - only been reported by Momma *et al.*^[32]. Ambient atmosphere storage conditions can also have an impact *via* the electrolyte on lithium ion batteries^[33] and LMBs^[34]. This field of research is especially relevant for Li||air batteries^[35,36], as this cell setup allows for an unlimited amount of oxygen to enter the battery during its lifetime. On the other hand, in the case of common research coin cell battery setups, the *in coin cell* atmosphere (ICCA, [Figure 1](#)) is limited to the volume of gas trapped inside the cell during crimping. The isolated impact of the ICCA has not been analyzed to date, despite it having an impact on the comparability of all obtained scientific results gathered using a coin cell setup. Furthermore, results generated within the confines of a glovebox (GB) ICCA might not be straightforwardly transferrable to industrial applications, since large-scale battery production is mostly conducted in clean and/or dry room (DR) atmospheres.

In an attempt to close this knowledge gap, we report on the significant impact of this remaining trapped ICCA on the chemical and electrochemical characteristics of lithium metal electrodes as well as the performance and lifetime of transition metals (NMC811) using LMBs by comparing a DR and a super-clean water-oxygen-nitrogen-free inert gas argon GB atmosphere. After precautions were taken to ensure safe storage conditions, thus ensuring equal starting conditions for each experiment, Li||Li and NMC811||Li cells were assembled in a GB and a DR. Stripping/Plating experiments, *operando* electrochemical impedance spectroscopy (EIS), *post-mortem* scanning electron microscopy (SEM), and X-ray photoelectron spectroscopy (XPS) analysis were conducted for Li||Li symmetric cells. The impact of the ICCA on LMB full cell performance was evaluated by galvanostatic cycling in NMC811||Li cells and subsequent *post-mortem* attenuated total reflection Fourier-transform infrared (ATR-FTIR) spectroscopy analysis of the CEI. In addition, based on the recorded ATR-FTIR analysis, a new decomposition mechanism of FEC on NMC811 was proposed and supported by different quantum chemistry calculations. Furthermore, the systematic analysis of two atmospheres with two additive-containing electrolytes and one baseline organic carbonate-based liquid electrolyte revealed a differently pronounced ICCA influence depending on the electrolyte formulation. The following electrolytes were chosen based on an equal molar approach: a baseline electrolyte [BE; EC:EMC 3:7 (w/w), 1.2 M LiPF₆] and two additive electrolytes containing the popular additives FEC (AE-FEC; BE +6.09 wt.% FEC) and VC (AE-VC; BE +5 wt.% VC)^[7].

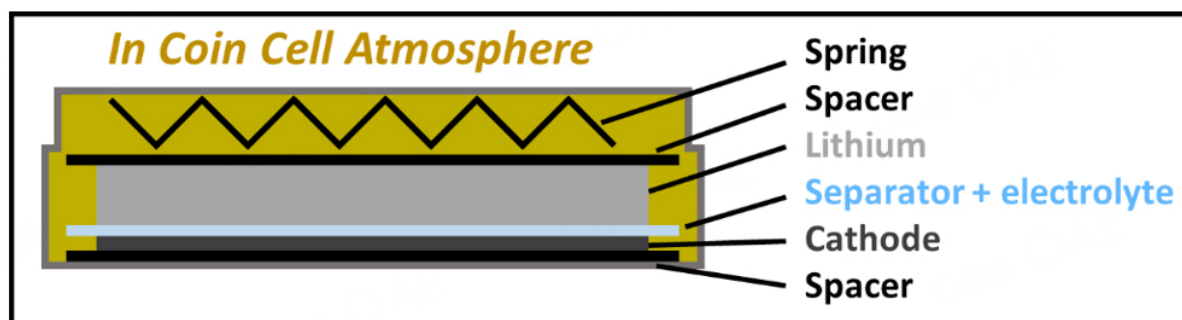


Figure 1. Schematic depiction of a coin cell 2032 setup commonly used in research, highlighting the available ICCA volume.

EXPERIMENTAL

Study design

The study presented in this work required careful preparation and considerable investment in experimental equipment to ensure that factors other than the ICCA trapped inside the battery did not have an impact on the experimental result. A major challenge of the experimental preparation is the ability to conduct all experiments with equal starting materials [Supplementary Figure 1A and B]. The aforementioned degradation of cathode materials and the reactivity of lithium metal with the atmosphere cannot be completely prevented by a standard GB atmosphere (H_2O and O_2 content < 1 ppm). Reactions of the starting materials with liquid electrolyte aerosols or chemicals stored in the same glovebox have an influence on the conducted analysis. In particular, the degradation of lithium metal with contaminations in an argon GB atmosphere (especially N_2) can result in black stains on lithium [Supplementary Figure 1C]. The native passivation layer covering battery-grade lithium^[7] and the degradation of battery-grade lithium in contact with nitrogen have received little attention in the past^[31]. This is despite the fact that the reaction of lithium and N_2 gas has previously been reported to form an artificial Li_3N -rich SEI^[37]. These degradations occur slowly due to the intended low amount of reaction partners in a standard argon-filled GB and the native passivation functioning as a protective film covering the elemental lithium metal on the inside. Once the native passivation layer is removed, for example, by cutting a rod of lithium with a tungsten wire, an accelerated reaction with nitrogen in the presence of trace amounts of oxygen results in an initially rainbow-colored and ultimately black reaction product surface containing nitrogen as a main component [Supplementary Figure 1D-H]. Working with lithium metal in a N_2 -filled glovebox is therefore not recommended.

For this study, a two-chamber GB was designed [Supplementary Figure 2] to store cathode and anode materials safely, preventing any degradation and thus ensuring comparable experimental results. One of the two chambers is only used to store commercially purchased cathodes and anodes. The electrodes intended for cell assembly were transferred to the second chamber through an antechamber, thus preventing electrode materials from ever coming into contact with the ambient atmosphere. Commercially purchased cathodes were only taken out of the GB during the drying process in an air-tight device. The GB is equipped with an additional solvent filter, an air conditioning system (set to 25°C), and a nitrogen purification system, preventing an increase of N_2 in a GB above 5 ppm. Coin cell parts and all other components (if possible) were extensively dried before being introduced into the GB. Coin cell parts and electrolytes intended for cell assembly in a DR (dew point $< -60^\circ\text{C}$) were packed in an air-tight transport device inside the GB whenever new cells needed to be assembled. During cell assembly inside the DR, the exposure of the

coin cell parts and electrodes to the DR atmosphere was kept to a minimum amount of time (< 10 min). Consequently, the ICCA trapped inside the assembled coin cells remained the only major influential difference in this study.

Materials

Lithium metal foil (Honjo Lithium GmbH., Ltd., 300 μm thickness, 99.9%) was stored in an argon-filled glovebox (MBraun Labmaster, H_2O and O_2 content < 0.1 ppm, N_2 content < 5 ppm). NMC811 electrodes with an active mass loading of 1.03 mAh cm^{-2} , purchased from Custom Cells, were dried at 120 $^\circ\text{C}$ in vacuum for at least 24 h before use and stored in an argon-filled glovebox (MBraun Labmaster, H_2O and O_2 content < 0.1 ppm, N_2 content < 5 ppm). All lithium metal and NMC811 electrodes used in this study originated from the one respective batch/sheet of battery grade lithium and NMC811 cathode material to achieve a high level of comparability for all conducted experiments.

The study utilized three organic carbonate-based electrolyte formulations. The baseline electrolyte (BE) [1.2 M LiPF_6 in EC:EMC 3:7 (w/w)] and the two film-forming additive-containing electrolytes AE-VC [1.2 M LiPF_6 in EC:EMC 3:7 (w/w) + 5 wt.% VC] and AE-FEC [1.2 M LiPF_6 in EC:EMC 3:7 (w/w) + 6.09 wt.% FEC], purchased from E-lyte Innovations GmbH, were used as received for coin cell 2032 assembly (for exact formulations, [Supplementary Tables 1-3](#)). The electrolytes were stored in an argon-filled glovebox (MBraun, H_2O and O_2 content < 0.1 ppm, N_2 content < 5 ppm).

Coin cell assembly

Two-electrode coin cell assembly was performed in an argon-filled glovebox (MBraun Labmaster, H_2O and O_2 content < 0.1 ppm, N_2 content < 5 ppm) or dry room (-60 $^\circ\text{C}$ dew point). The exact procedure for cell assembly in the dry room is discussed in the “study design” chapter of the experimental section. In each coin cell, electrodes with a 12 mm diameter, an electrolyte volume of 30 μL with one layer of Celgard 2500 (16 mm diameter), and two 0.5 mm stainless steel spacers were used to form the battery stack shown in [Figure 1](#).

Stripping/Plating and galvanostatic cycling experiments

Stripping/Plating experiments of $\text{Li}||\text{Li}$ symmetric cells and galvanostatic cycling of NMC811 $||\text{Li}$ cells were conducted at 20 $^\circ\text{C}$ using a MACCOR battery cycler (MACCOR Series 4000).

Stripping/Plating experiments in $\text{Li}||\text{Li}$ cells were carried out for 1,000 charge/discharge cycles at a constant current of 0.5 mA cm^{-2} , with one-hour stripping/plating steps (0.5 mAh cm^2). Galvanostatic cycling in NMC811 $||\text{Li}$ cells was carried out at a constant current density of 0.5 mA cm^2 (equivalent to $\sim C/2$, based on an areal capacity of 1.03 mAh cm^{-2}) in the voltage range of 3 V to 4.2 V. Prior to the experiment, each cell was allowed to rest for 12 h.

Operando electrochemical impedance spectroscopy

Operando electrochemical impedance spectroscopy (EIS) measurements were carried out at a BioLogic VMP3 workstation. A $\text{Li}||\text{Li}$ symmetric cell was cycled 50 times (charged and discharged for 1 h each at 0.5 mA/cm^2) and the impedance was measured every 5 cycles (10 h). The data of the measured Nyquist plots were evaluated and fitted with BioLogic’s EC-Lab software using an equivalent circuit selection of $R_1 + Q_2/R_2 + Q_3/R_3$.

Post-mortem sample preparation

Electrodes intended for *post-mortem* analysis (SEM, XPS, ATR-FTIR) were harvested from coin cells which were opened in an argon-filled glovebox (MBraun, H_2O and O_2 content < 0.1 ppm, N_2 content < 5 ppm).

The electrodes were rinsed with ethyl methyl carbonate (EMC; E-Lyte Innovations; $3 \times 500 \mu\text{L}$) and subsequently dried in an antechamber for > 15 min. They were then transported to the workstations or measurement devices using in-house-built (SEM, ATR-FTIR) or commercially available (XPS, Vacuum Transfer module by Thermo Scientific) sample transfer holders, preventing any contact with the outer atmosphere and/or moisture.

Scanning electron microscopy

Scanning electron microscopy (SEM) measurements were conducted at a Carl Zeiss Auriga Modular Crossbeam workstation utilizing a Schottky field emission gun with a Gemini column as an electron source. Images were taken at an accelerating voltage of 3 kV (SEM) using an in-lens secondary electron detector. The aperture of the lens was $20 \mu\text{m}$ and the working distance was 3.0 mm.

X-ray photoelectron spectroscopy

X-ray photoelectron spectroscopy (XPS) measurements were carried out at an angle of emission of 0° and a pass energy of 20 eV using a monochromatic Al $K\alpha$ source ($E_{\text{photon}} = 1,486.6 \text{ eV}$) with a 10 mA filament current and a filament voltage source of 12 kV. The analyzed area was approximately $300 \mu\text{m} \times 700 \mu\text{m}$. In order to compensate for the charging of the sample, a charge neutralizer was used. The F 1s peak at 684.8 eV (LiF) was taken as an internal reference for the adjustment of the energy scale in the spectra. CasaXPS software was used for fitting and peak assignment in accordance with known literature values^[38,39].

Attenuated total reflection Fourier transform infrared spectroscopy

Attenuated total reflection Fourier transform infrared spectroscopy (ATR-FTIR) analysis of the CEI on NMC811 electrode surfaces was conducted on a Bruker ALPHA II FT-IR spectrometer with a platinum ATR unit (diamond crystal) and a DLaTGS detector inside an argon-filled glovebox (H_2O and $\text{O}_2 < 5 \text{ ppm}$). ATR-FTIR measurements were conducted at multiple spots in the center, the middle and the edge of the harvested electrode [Supplementary Figure 3]. The spectra were acquired with a spectral resolution of 4 cm^{-1} at an incidence angle of 45° . Each spectrum was obtained by accumulating 32 and 64 interferograms for background and sample spectra, respectively. The spectra are presented in the form of absorbance and were processed by subtracting the spectrum of pristine NMC811, ATR correction, and concave rubber band correction (10 iterations, straight lines).

Quantum chemistry calculations

Different quantum chemistry methods were used to interpret experimental results and to propose a new decomposition mechanism for FEC on NMC811 electrode. Density functional theory (DFT) calculations of putative decomposition products were performed at the B3LYP/6-311+G (3df, 2p) level of theory^[40-42] using Grimme's empirical D3 dispersion correction with Becke-Johnson damping^[43]. In addition, reaction energies and free energies, as well as the corresponding barriers, were calculated using the highly accurate G4MP2 composite method^[44]. All calculations were performed using the Gaussian 16 software using the SMD solvation model with acetone parameters^[45].

RESULTS AND DISCUSSION

Stripping/Plating and *operando* EIS performed in Li||Li symmetric cell setups

Initial electrochemical characterization to determine the influence of the ICCA on lithium metal electrodes was conducted by stripping/plating experiments [Figure 2] in Li||Li symmetric cells at a constant current density of 0.5 mA cm^{-2} (0.5 mAh cm^{-2}) until the cell reached a set limit of $\pm 0.3 \text{ V}$. The eventual increase in overvoltage values originates from a reduced Li transport in the electrolyte due to the consumption of Li^+ ion transporting components. Utilizing a Li||Li symmetric cell setup allows the effect of the different ICCAs to be narrowed down to the impact on the lithium metal electrode and excludes the influences of

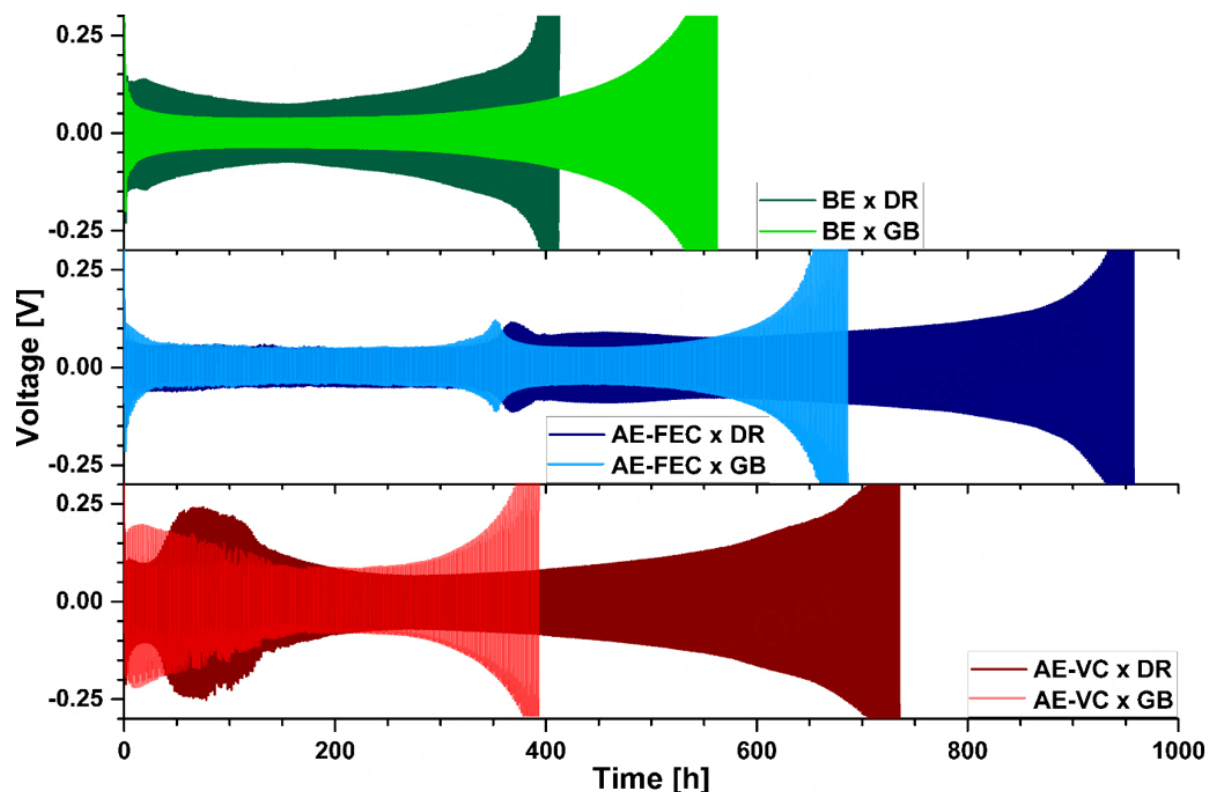


Figure 2. Voltage vs. time profiles (0.5 mA cm^{-2} , 1 h charge and discharge) of six different Li||Li cell setups. Top: BE \times DR - dark green, BE \times GB - light green; middle: AE-FEC \times DR - dark blue; AE-FEC \times GB - light blue; bottom: AE-VC \times DR - dark red; AE-VC \times GB - light red.

intercellular crosstalk^[46,47]. Six different cell setups were characterized and analyzed, each containing an individual combination of atmosphere (GB, DR) and electrolyte (BE, AE-FEC, AE-VC), and will be referred to hereafter as: electrolyte \times atmosphere (e.g., BE \times DR or AE-VC \times GB).

The different atmospheres result in different stripping/plating (voltage vs. time) profiles for all three electrolyte containing cells. The BE \times DR cell setup (top) experiences increased overvoltage values ($> 75 \text{ mV}$), which never decrease to the values of BE \times GB (50 mV) and have a less homogeneous shape [Supplementary Figure 4], indicating inhomogeneous stripping/plating^[48] as well as increased dendrite growth^[49]. The stripping/plating experiments of the AE-FEC-containing cells result in similar overvoltage profiles for both atmospheres for the first 350 h. The short-term overvoltage value increase (350-400 h) is believed to be caused by the complete consumption of FEC in the considered electrolyte^[50], after which the overvoltage profiles start to differentiate. Based on these results, it is assumed that the ICCA does not influence the rate of FEC consumption. However, it might still affect the decomposition products and resulting chemical composition of the *in situ* formed SEL, resulting in a different overvoltage profile after FEC consumption. The most significant difference in electrochemical characteristics was recorded for the cell setups containing AE-VC. Whereas AE-VC \times GB experiences high overvoltage values ($\pm 0.25 \text{ V}$) during the initial cycles, the DR ICCA in AE-VC \times DR results in reduced values ($\pm 0.1 \text{ V}$) for the first 40 h. The values for AE-VC \times DR subsequently start to increase and reach the same values as the GB-containing counterparts after 50 cycles. Thereafter, the overvoltage values increase further and reach a local maximum after 75-80 h. These results indicate that the DR ICCA alters the reactivity of some AE-VCs components on lithium metal. Lifetime comparisons of stripping/plating experiments in Li||Li symmetric cells are not as

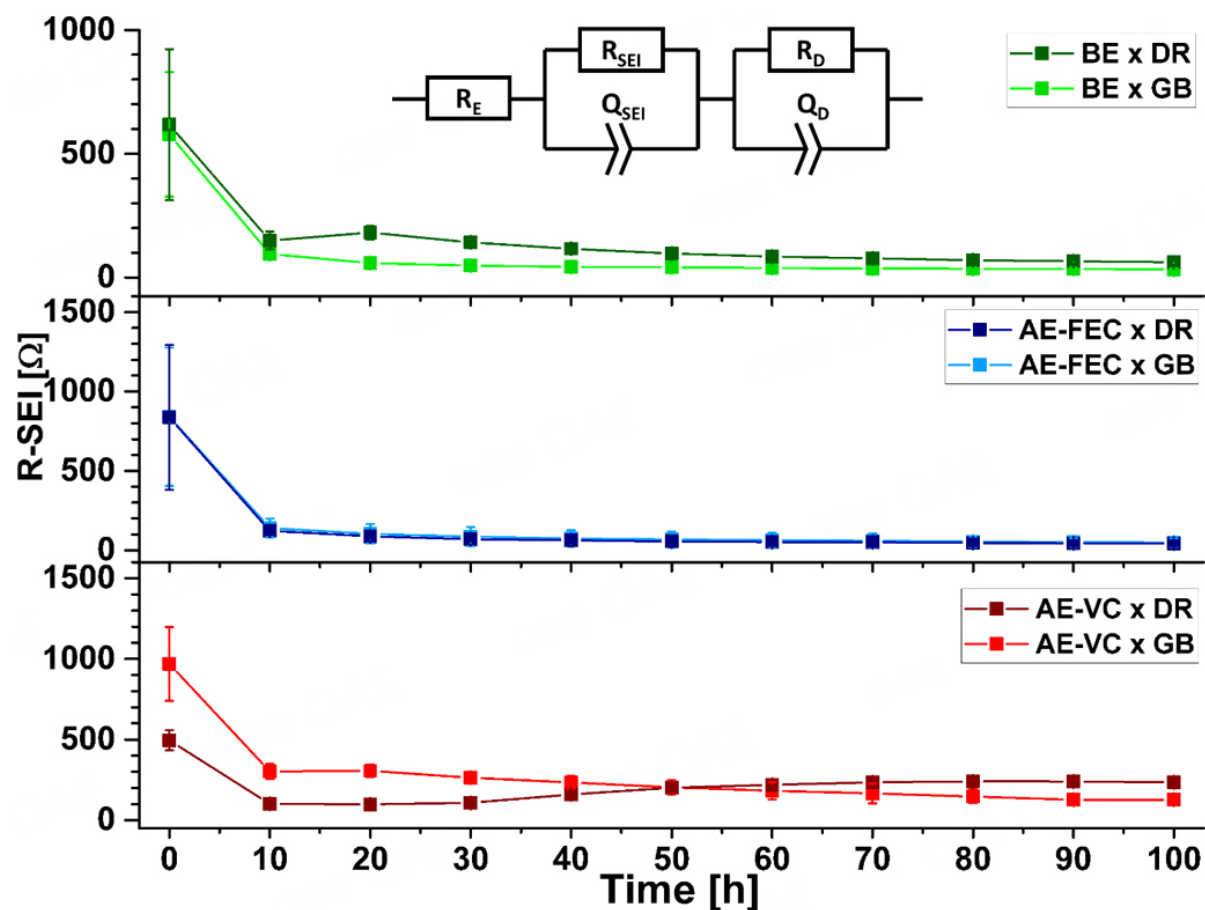


Figure 3. R_{SEI} measured over the initial 100 h of stripping/plating experiments (0.5 mA cm^{-2} , 1 h stripping/plating), based on a Nyquist plot fitted by the insert RC equivalent circuit. Values depict an average of at least five measurements with the error corresponding to the standard deviation between the measured values. Top: BE x DR - dark green; BE x GB - light green; middle: AE-FEC x DR - dark blue; AE-FEC x GB - light blue; bottom: AE-VC x DR - dark red, AE-VC x GB - light red.

reproducible as they are for LMB full cells. Nevertheless, it was observed that the lifetime of the experiment differed for all three electrolytes depending on the ICCA. Notably, BE x GB outperformed BE x DR, whereas the cells containing DR ICCA outperformed their GB analogues for both additive-containing electrolytes, thus indicating the significant impact of additive reactivity on lithium metal-based battery cell setups. Additional stripping/plating experiments comparing the nitrogen-free GB atmosphere to a standard argon-filled glovebox (Ar-GB; without a nitrogen purification system) revealed little differences in overvoltage values, indicating a limited partial impact of N_2 on *in cell* reactivity [Supplementary Figure 5]. Furthermore, forcing a reaction of lithium with the different atmospheres (DR and GB) by generating a fresh lithium surface *via* known procedures^[7,39] followed by cell assembly in a GB only showed a minimal impact on stripping/plating performance [Supplementary Figure 6] compared to that of the ICCA.

Differences in overvoltage have a strong correlation to the resistance of the SEI (R_{SEI})^[48,51]. The first 100 h of the stripping/plating experiment were therefore investigated further utilizing *operando* EIS [Figure 3]. Additional stripping/plating experiments of identical cell setups were galvanostatically cycled for 100 h at 0.5 mA cm^{-2} and impedance spectra were recorded every 10 h. The measured, fitted, and averaged results show the characteristic drop in SEI resistance (R_{SEI}) after the initial cycles, which is likely caused by the replacement of the native passivation layer by an *in situ* formed SEI^[7]. After the initial drop, the evolution of

the R_{SEI} values closely mimics the overvoltage evolution of the stripping/plating experiments: The R_{SEI} values of the BE \times DR setup remain higher compared to the BE \times GB setup counterparts and both AE-FEC containing cell setups show similar R_{SEI} values over the first 100 h. The drastic difference in the overvoltage evolution of the stripping/plating experiments for AE-VC \times DR and AE-VC \times GB can also be seen in the evolution of the R_{SEI} values. Initially, AE-VC \times GB experiences a higher SEI resistance, but after 30 h, the resistance of the AE-VC \times DR starts to rise and matches the shrinking AE-VC \times GB values after 50 h. The R_{SEI} values of AE-VC \times DR subsequently reach a local maximum at 80-90 h before they gradually start to shrink, as is the case for the overvoltage values of the stripping/plating experiments.

Overall, the stripping/plating experiments and *operando* EIS measurements show the notable influence of the ICCA on the electrochemical characteristics of the SEI. In the case of both BE and AE-VC, the ICCA has a strong impact on the overvoltage profiles and R_{SEI} . However, the influence on the R_{SEI} of FEC containing cells seems to be minimal, although different overvoltage values of AE-FEC \times DR and AE-FEC \times GB after FEC consumption indicate different decomposition products depending on the ICCA. The observed influences could originate from different chemical compositions of the SEI depending on the ICCA and could result in different stripping/plating homogeneity.

Post-mortem analysis of Li||Li symmetric cells

Electrochemical characterization revealed that the ICCA has an influence on the performance of lithium metal electrodes. In line with this, *post-mortem* SEM and XPS analysis after 100 h were performed to observe the differences in stripping/plating homogeneity and determine how the ICCA influences the chemical composition of the *in situ* formed SEI on the lithium metal.

Post-mortem SEM measurements [Figure 4A-F], in combination with optical analysis of the complete harvested electrode (inlets), enable an evaluation of the stripping/plating homogeneity of lithium metal electrodes. Electrochemical characterization only revealed a small impact of different ICCAs on the first 100 h in combination with AE-FEC, some impact with BE, and a strong impact in combination with AE-VC, which can also be observed after cell disassembly. The lower overvoltage profiles and R_{SEI} values of BE \times GB [Figure 4A] coincide with pronounced stripping/plating (black/gray spots) taking place on the electrode surface and less concentrated stripping/plating around the edges of the electrode, as is the case for its DR [Figure 4B] counterpart. In the case of the cell setups containing functional additives, the electrodes harvested from AE-FEC \times GB [Figure 4C] and AE-FEC \times DR [Figure 4D] look very similar. The most substantial differences were observed for the cells containing AE-VC. Electrodes harvested from AE-VC \times GB [Figure 4E] showed indications of stripping/plating over the whole electrode surface, whereas stripping/plating of AE-VC \times DR [Figure 4F] almost exclusively takes place around the electrode edges. A previous publication suggested a correlation of a lower R_{SEI} value and an increased stripping/plating homogeneity^[7], which is in agreement with the findings of this study for BE and AE-VC after 100 h. In the case of AE-FEC, the passivating reactivity of FEC appears to suppress the impact of different ICCAs on stripping/plating homogeneity after 100 h.

The chemical composition of the SEI formed on the lithium metal electrode after 100 h was analyzed *via post-mortem* XPS analysis [Figure 4G]. In an attempt to only look at the *in situ* formed SEI, only spots that clearly experienced stripping/plating processes (black spots, see Figure 4A-F) were analyzed and the results were subsequently averaged. For all three electrolytes, considerable differences in the atomic distributions of the *in situ* formed SEI were found depending on the ICCA and they all contained the expected mixture of organic, carbonate, fluoride, and phosphate components^[7,39]. For BE, a higher carbon content (BE \times GB: 21%; BE \times DR: 25%) and a slightly lower fluorine content (BE \times GB: 38%; BE \times DR: 35%) were observed. In

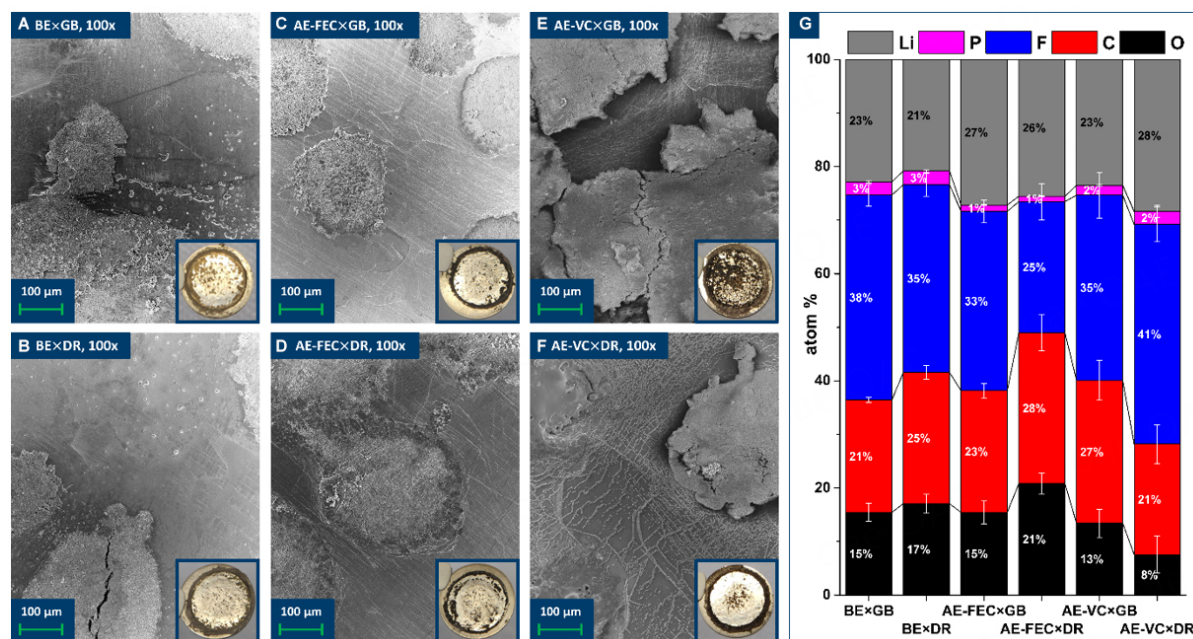


Figure 4. Post-mortem SEM (A-F) and XPS (G) analyses of Li||Li cells after 50 cycles at 0.5 mA cm^{-2} (0.5 mAh cm^{-2}). Post-mortem SEM and optical (inlets) images of electrodes harvested from (A) BE × GB, (B) BE × DR, (C) AE-FEC × GB, (D) AE-FEC × DR, (E) AE-VC × GB, and (F) AE-VC × DR, and atomic distribution of *in situ* formed SEIs of the same cell setups calculated and averaged by XPS analysis (G).

the case of AE-FEC, the *in situ* formed SEI contains more oxygen (AE-FEC × GB: 15%; AE-FEC × DR: 21%) and carbon (AE-FEC × GB: 23%; AE-FEC × DR: 28%), but notably less fluorine (AE-FEC × GB: 33%; AE-FEC × DR: 25%). These findings show that the similar results of the electrochemical characterizations of AE-FEC × GB and AE-FEC × DR over the first 100 h [Figures 2 and 3] do not automatically equate to an equal *in situ* formed SEI composition and support the hypothesis that the different long cycle life after complete FEC consumption might be caused by a different SEI composition. XPS analysis of the cells containing AE-VC shows opposite tendencies compared to AE-FEC. The *in situ* formed SEI in AE-VC × GB has higher oxygen (AE-VC × GB: 15%; AE-VC × DR: 8%) and carbon content (AE-VC × GB: 28%; AE-VC × DR: 21%) but a considerably lower fluorine content (AE-VC × GB: 33%; AE-VC × DR: 41%). For all three electrolytes, a correlation between the carbon and oxygen content of the SEI is observable: For both BE × DR and AE-FEC × DR, the oxygen and carbon contents are higher compared to their GB analogues. This trend is reversed for AE-VC and could be the result of a different VC reactivity with oxygen compared to FEC and the BE electrolyte components [Supplementary Figure 7]. This correlation also explains the limited impact of the different ICCAs on the individual chemical species distribution of the *in situ* formed SEI [Supplementary Figure 8]. As was the case for the electrochemical characterization and post-mortem SEM analysis, the *in situ* formed SEI in cell setups containing AE-VC are impacted most by the different ICCAs. Overall, post-mortem analysis after 100 h suggests that the ICCA has an impact on stripping/plating homogeneity after 100 h, in the case of BE and AE-VC, and a considerable influence on the compositions of *in situ* formed SEI in Li||Li symmetric cells.

Galvanostatic cycling performance in NMC811||Li cells

This study has so far focused on the influence of the ICCA on the lithium metal electrode. In the following section, the influence of the ICCA on NMC811||Li full cell setups will be analyzed by galvanostatic cycling at a constant current density of 0.5 mA cm^{-2} ($\sim C/2$, areal cathode capacity: 1.03 mAh cm^{-2}). As with all the lithium electrodes used, all NMC811 electrodes originated from one NMC811 electrode sheet to achieve a

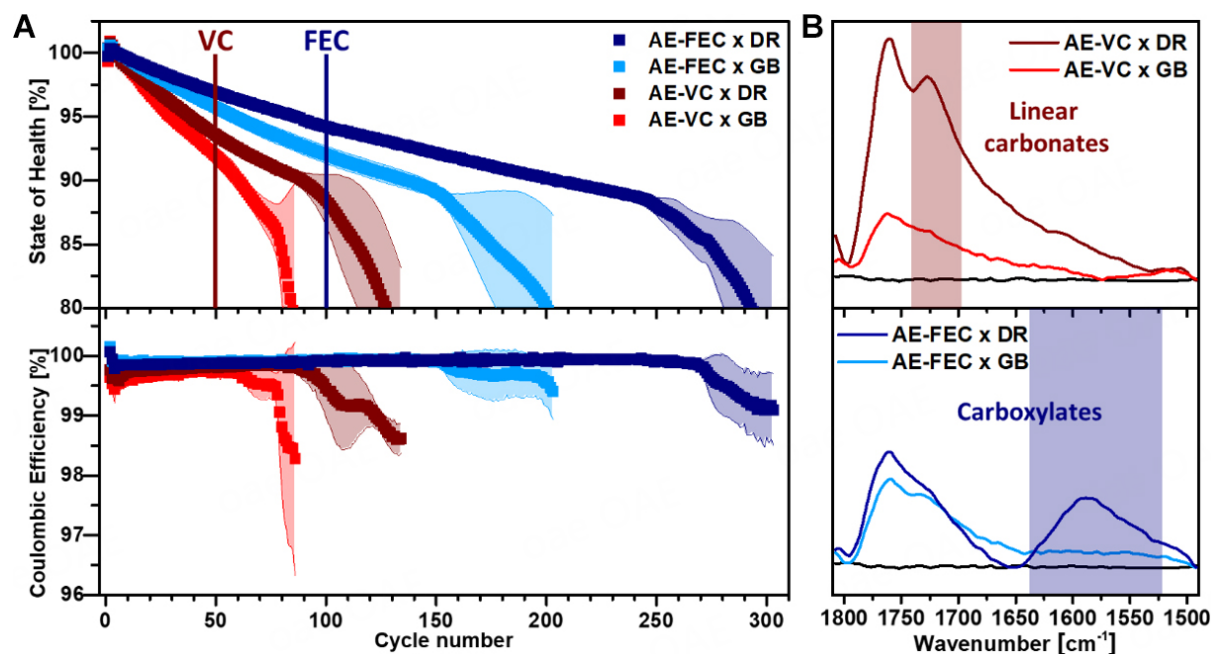
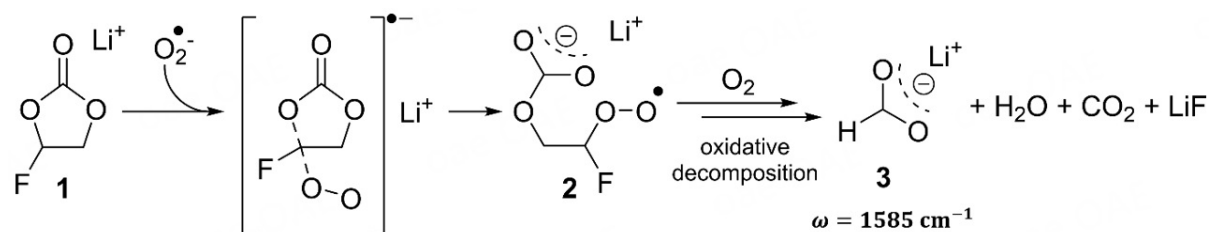


Figure 5. (A) SOH and CE profiles of NMC811||Li cells at a constant current density of 0.5 mA h cm^{-2} between 4.2 V and 3.0 V ($-C/2$, areal cathode capacity: $1.03 \text{ mA h cm}^{-2}$). Top: SOH; bottom: CE. The presented results are an average of three cell setups of each kind. (B) *Post-mortem* IR analysis of the CEI on NMC811 cathodes after 50 cycles (AE-VC, top) and 100 cycles (AE-FEC, bottom). AE-FEC \times DR - dark blue; AE-FEC \times GB - light blue, AE-VC \times DR - dark red, AE-VC \times GB - light red, NMC811 baseline - black.

high level of comparability. Since the functional additives considered were shown to be indispensable electrolyte components for LMB performance^[7,52], only AE-FEC and AE-VC will be discussed going forward. The same nomenclature will be used in the report hereafter, although one Li electrode was exchanged with a NMC811 cathode.

The recorded galvanostatic cycling data were investigated based on the average state of health (SOH, normalized on the 5th cycle) and the Coulombic efficiency. The advantage of FEC over VC as a film-forming additive for the analyzed cell setup has been reported previously^[7]. However, to the best of our knowledge, there are no reports on the influences of the ICCA on additive comparability, especially with regard to cell lifetime (end-of-life (EOL) criteria: 80% SOH). For both additive-containing electrolytes analyzed, the lifetime of the LMB was notably enhanced by a DR ICCA [Figure 5A]. In the case of the cell setup containing the VC additive, the average lifetime increases by +50% from 85 cycles in the case of AE-VC \times GB to 128 cycles for AE-VC \times DR. In the case of AE-FEC, the overall average lifetime increases by 93 cycles (+46%) by AE-FEC \times GB (201 cycles) to AE-FEC \times DR (294 cycles) is arguably even more significant. Furthermore, the GB ICCA seems to lead to a less consistent cycle life. For both AE-VC \times GB and AE-FEC \times GB, the starting point of the roll-over (= “sudden death”) effect has a higher variance, which is illustrated by the larger error after the rollover effect has started compared to the DR-containing analogues. The ICCA also has an influence on the CE of the cell setups. Over the first 50 cycles (until the start of AE-VC \times GB rollover effect), the average CE of AE-VC \times DR (99.765%) is 0.085% higher compared to AE-VC \times GB (99.680%), which is a significant margin in the aim of reaching 99.9% CE^[52]. In the case of FEC containing cells, the average CE difference over the first 150 cycles is less pronounced (0.024%).

To determine the origin of the enhanced full cell performance, the CEIs chemical composition on NMC811 electrode was analyzed by means of *post-mortem* ATR-FTIR spectroscopy [Figure 5B] after 50 cycles



Scheme 1. Proposed oxidative decomposition mechanism for FEC (1) in the presence of oxygen as part of the formation of CEI, based on FTIR analysis, quantum chemistry calculations, and known literature^[56-59]. The stated IR band was determined *via* DFT calculations for the carbonyl bond of lithium formate (3).

(AE-VC × GB and AE-VC × DR) and 100 cycles (AE-FEC × GB and AE-FEC × DR). The number of cycles was chosen in a way that ensured a notable difference in the SOH of the cells but also that it would not be influenced by the roll-over effect. For the VC-containing cells, a relatively more intense band generally associated with linear carbonates (1,740-1,700 cm^{-1}) was observed for AE-VC × DR in relation to that of cyclic and poly-cyclic carbonate compounds (1,790-1,740 cm^{-1})^[53-55]. In the case of the FEC containing cell setup, a new band (1,630-1,540 cm^{-1}) was observed in the presence of the DR ICCA (AE-FEC × DR), indicating the formation of lithium carboxylates. The same band was not detected for AE-FEC × GB. Furthermore, the amounts of linear carbonates for AE-VC × DR and carboxylates for AE-FEC × DR were more pronounced at the edges of the electrodes compared to the center of the electrode [Supplementary Figure 3]. This observation is explained by the easier access of the ICCA to the cathode at the edges of the battery stack than at its center, and might also indicate an inhomogeneous de-/intercalation behavior of the cathode.

Since the new carboxylate band (1,600-1,570 cm^{-1}) is only detected for the AE-FEC × DR cell setup, its compound origin has to be formed in a reaction involving FEC and, most likely, oxygen. For Li||O₂ batteries, a decomposition mechanism of propylene carbonate to carboxylates in the presence of oxygen was proposed by Freunberger *et al.*^[56]. A similar oxidative decomposition mechanism of FEC might be feasible and was supported by quantum chemical calculations [Scheme 1]. The energy barriers for a nucleophilic attack of a superoxide radical onto FEC (1) show a tendency towards a ring-opening reaction over a C-F bond cleavage (ring opening: 9.8 kcal mol^{-1} ; C-F bond cleavage: 11.8 kcal mol^{-1} , see Supplementary Figure 9). This attack would result in the formation of an intermediate peroxo radical (2)^[57], which could further decompose into lithium formate (3) in the presence of excess oxygen^[58,59]. The calculated IR band of the proposed lithium formate (1,585 cm^{-1}) and previously reported FTIR measurements^[56] support the proposed mechanism. As an analogue product to lithium acetate of the propylene carbonate mechanism^[56], lithium fluoroformate would readily decompose into LiF and CO₂. A similar decomposition mechanism for VC is unlikely, because a quantum chemical calculation determined unfavorable reaction energies for the nucleophilic attack of the superoxide radical onto the electron-rich C=C double bond [Supplementary Figure 7].

Overall, the ICCA was shown to have a very high impact on the lifetime and CE of the analyzed LMBs, which is likely caused by a varying CEI composition. In both cases, the NMC811||Li cells containing DR ICCA outperform the cell lifetime of their GB analogues by an average of 46% (FEC) and 50% (VC) until 80% SOH. *Post-mortem* ATR-FTIR analysis of the respective cathodes revealed a more pronounced formation of linear carbonates for AE-VC × DR cell setups and the formation of carboxylates for AE-FEC × DR cell setups, which are noteworthy alterations compared to the GB analogues. Furthermore, the different accessibility of the ICCA to different parts of the battery stack leads to an inhomogeneous chemical composition of the CEI.

CONCLUSION

The two different ICCAs (GB and DR) were found to have a substantial impact on the coin cell performance of the LMB, originating from the altered interphase compositions of the SEI and CEI covering the lithium metal anode and NMC₈₁₁ cathode, respectively. Furthermore, the effect of the ICCA itself was differently pronounced depending on the film-forming electrolyte additives VC or FEC. However, both additive-containing electrolytes were shown to form performance-enhancing chemical CEI compositions with a DR ICCA. Stripping/Plating experiments and *operando* EIS analysis also revealed that the ICCA has a considerable impact on overvoltage *vs.* time profiles and R_{SEI} values for Li||Li symmetric cells containing BE and AE-VC. Differences in stripping/plating homogeneity were observed by *post-mortem* optical analysis (incl. SEM imaging) for different ICCAs and electrolytes, while *post-mortem* XPS analysis revealed different atomic SEI compositions for all three considered electrolyte formulations. In the case of NMC₈₁₁||Li full cell setups, the DR ICCA resulted in a reduced capacity fade and delayed rollover effect, ultimately leading to an increased lifetime (EOL: 80% SOH) for both AE-VC and AE-FEC of up to 50%. This enhancement is the result of a modified CEI composition, containing more linear carbonates in the case of AE-VC × DR and the formation of carboxylates for AE-FEC × DR, which was revealed by *post-mortem* ATR-FTIR analysis. Based on the FTIR analysis, a new oxidative decomposition mechanism for FEC in the presence of oxygen was proposed and supported by quantum chemical calculations, revealing lithium formate as the newly formed CEI component. In particular, the formation of new chemical components and overall impacted electrolyte interphase compositions of anode (SEI) and cathode (CEI) demonstrates the previously underestimated impact of the ICCA as a highly influential factor for the comparability of research results as well as the transfer of research knowledge to industrial application for future LMBs.

DECLARATIONS

Authors' contributions

Methodology, investigation, formal analysis, writing (original draft): Kühn SP

Investigation, formal analysis: Weiling M, Diddens D

Formal analysis, writing (review & editing): Baghernejad M

Writing (review & editing), supervision: Winter M

Conceptualization, supervision, writing (review & editing): Cekic-Laskovic I

Availability of data and materials

Data will be made available on request.

Financial support and sponsorship

The authors are grateful for the financial support provided within the LILLINT project (13XP0225B) funded by the German Federal Ministry of Education and Research (BMBF).

Conflicts of interest

All authors declared that there are no conflicts of interest.

Ethical approval and consent to participate

Not applicable.

Consent for publication

Not applicable.

Copyright

© The Author(s) 2023.

REFERENCES

1. Winter M, Barnett B, Xu K. Before Li ion batteries. *Chem Rev* 2018;118:11433-56. DOI PubMed
2. Zhang JG, Xu W, Xiao J, Cao X, Liu J. Lithium metal anodes with nonaqueous electrolytes. *Chem Rev* 2020;120:13312-48. DOI
3. Xu K. Electrolytes and interphases in Li-ion batteries and beyond. *Chem Rev* 2014;114:11503-618. DOI PubMed
4. Bieker P, Winter M. Was braucht man für eine super-batterie? *Chemie Unserer Zeit* 2016;50:26-33. DOI
5. Xu K. Nonaqueous liquid electrolytes for lithium-based rechargeable batteries. *Chem Rev* 2004;104:4303-417. DOI PubMed
6. Horstmann B, Shi J, Amine R, et al. Strategies towards enabling lithium metal in batteries: interphases and electrodes. *Energy Environ Sci* 2021;14:5289-314. DOI
7. Kühn SP, Pfeiffer F, Bela M, et al. Back to the basics: advanced understanding of the as-defined solid electrolyte interphase on lithium metal electrodes. *J Power Sources* 2022;549:232118. DOI
8. Peled E. The electrochemical behavior of alkali and alkaline earth metals in nonaqueous battery systems - the solid electrolyte interphase model. *J Electrochem Soc* 1979;126:2047-51. DOI
9. Peled E, Menkin S. Review - SEI: past, present and future. *J Electrochem Soc* 2017;164:A1703-19. DOI
10. Jie Y, Ren X, Cao R, Cai W, Jiao S. Advanced liquid electrolytes for rechargeable Li metal batteries. *Adv Funct Mater* 2020;30:1910777. DOI
11. Yang H, Guo C, Naveed A, et al. Recent progress and perspective on lithium metal anode protection. *Energy Stor Mater* 2018;14:199-221. DOI
12. Xia L, Miao H, Zhang C, Chen GZ, Yuan J. Review - recent advances in non-aqueous liquid electrolytes containing fluorinated compounds for high energy density lithium-ion batteries. *Energy Stor Mater* 2021;38:542-70. DOI
13. Yasin G, Arif M, Mehtab T, et al. Understanding and suppression strategies toward stable Li metal anode for safe lithium batteries. *Energy Stor Mater* 2020;25:644-78. DOI
14. Delaporte N, Wang Y, Zaghbi K. Pre-treatments of lithium foil surface for improving the cycling life of Li metal batteries. *Front Mater* 2019;6:267. DOI
15. Zhou H, Yu S, Liu H, Liu P. Protective coatings for lithium metal anodes: recent progress and future perspectives. *J Power Sources* 2020;450:227632. DOI
16. Gao S, Sun F, Liu N, Yang H, Cao P. Ionic conductive polymers as artificial solid electrolyte interphase films in Li metal batteries - a review. *Mater Today* 2020;40:140-59. DOI
17. Kang D, Xiao M, Lemmon JP. Artificial solid-electrolyte interphase for lithium metal batteries. *Batteries Supercaps* 2021;4:445-55. DOI
18. Li Y, Wang C, Gao R, Cao F, Ye H. Recent smart lithium anode configurations for high-energy lithium metal batteries. *Energy Stor Mater* 2021;38:262-75. DOI
19. Zhan Y, Shi P, Zhang X, et al. The insights of lithium metal plating/stripping in porous hosts: progress and perspectives. *Energy Technol* 2021;9:2000700. DOI
20. Cheng Y, Chen J, Chen Y, et al. Lithium host: advanced architecture components for lithium metal anode. *Energy Stor Mater* 2021;38:276-98. DOI
21. Zhou Y. External pressure: an overlooked metric in evaluating next-generation battery performance. *Curr Opin Electrochem* 2022;31:100916. DOI
22. Fang C, Lu B, Pawar G, et al. Pressure-tailored lithium deposition and dissolution in lithium metal batteries. *Nat Energy* 2021;6:987-94. DOI
23. Xiao J, Li Q, Bi Y, et al. Understanding and applying coulombic efficiency in lithium metal batteries. *Nat Energy* 2020;5:561-8. DOI
24. Adams BD, Zheng J, Ren X, Xu W, Zhang J. Accurate determination of coulombic efficiency for lithium metal anodes and lithium metal batteries. *Adv Energy Mater* 2018;8:1702097. DOI
25. Dai F, Cai M. Best practices in lithium battery cell preparation and evaluation. *Commun Mater* 2022;3:64-70. DOI
26. Song W, Harlow J, Logan E, et al. A systematic study of electrolyte additives in single crystal and bimodal $\text{LiNi}_{0.8}\text{Mn}_{0.1}\text{Co}_{0.1}\text{O}_2$ /graphite pouch cells. *J Electrochem Soc* 2021;168:090503. DOI
27. Harlow JE, Ma X, Li J, et al. A wide range of testing results on an excellent lithium-ion cell chemistry to be used as benchmarks for new battery technologies. *J Electrochem Soc* 2019;166:A3031-44. DOI
28. Sicklinger J, Metzger M, Beyer H, Pritzl D, Gasteiger HA. Ambient storage derived surface contamination of NCM811 and NCM111: performance implications and mitigation strategies. *J Electrochem Soc* 2019;166:A2322-35. DOI
29. Li Y, Li Y, Sun Y, et al. Revealing nanoscale passivation and corrosion mechanisms of reactive battery materials in gas environments. *Nano Lett* 2017;17:5171-8. DOI
30. Otto S, Moryson Y, Krauskopf T, et al. In-depth characterization of lithium-metal surfaces with XPS and ToF-SIMS: toward better understanding of the passivation layer. *Chem Mater* 2021;33:859-67. DOI
31. Otto S, Fuchs T, Moryson Y, et al. Storage of lithium metal: the role of the native passivation layer for the anode interface resistance in solid state batteries. *ACS Appl Energy Mater* 2021;4:12798-807. DOI

32. Momma T, Nara H, Yamagami S, Tatsumi C, Osaka T. Effect of the atmosphere on chemical composition and electrochemical properties of solid electrolyte interface on electrodeposited Li metal. *J Power Sources* 2011;196:6483-7. DOI
33. Bläubaum L, Röse P, Schmidt L, Krewer U. The effects of gas saturation of electrolytes on the performance and durability of lithium-ion batteries. *ChemSusChem* 2021;14:2943-51. DOI PubMed PMC
34. Stark JK, Ding Y, Kohl PA. Role of dissolved gas in ionic liquid electrolytes for secondary lithium metal batteries. *J Phys Chem C* 2013;117:4980-5. DOI
35. Wang E, Dey S, Liu T, Menkin S, Grey CP. Effects of atmospheric gases on Li metal cyclability and solid-electrolyte interphase formation. *ACS Energy Lett* 2020;5:1088-94. DOI PubMed PMC
36. Haas R, Murat M, Weiss M, Janek J, Natan A, Schröder D. Understanding the transport of atmospheric gases in liquid electrolytes for lithium - air batteries. *J Electrochem Soc* 2021;168:070504. DOI
37. Zhang Y, Wang W, Tang H, et al. An *ex-situ* nitridation route to synthesize Li₃N-modified Li anodes for lithium secondary batteries. *J Power Sources* 2015;277:304-11. DOI
38. Ding F, Xu W, Chen X, et al. Effects of carbonate solvents and lithium salts on morphology and coulombic efficiency of lithium electrode. *J Electrochem Soc* 2013;160:A1894-901. DOI
39. Becking J, Gröbmeyer A, Kolek M, et al. Lithium-metal foil surface modification: an effective method to improve the cycling performance of lithium-metal batteries. *Adv Mater Interfaces* 2017;4:1700166. DOI
40. Becke AD. Density-functional thermochemistry. III. The role of exact exchange. *J Chem Phys* 1993;98:5648-52. DOI
41. Krishnan R, Binkley JS, Seeger R, Pople JA. Self-consistent molecular orbital methods. XX. A basis set for correlated wave functions. *J Chem Phys* 1980;72:650-4. DOI
42. Mclean AD, Chandler GS. Contracted gaussian basis sets for molecular calculations. I. second row atoms, Z = 11-18. *J Chem Phys* 1980;72:5639-48. DOI
43. Allouche R. Gabedit - a graphical user interface for computational chemistry softwares. *J Comput Chem* 2010;32:174-82. DOI
44. Curtiss LA, Redfern PC, Raghavachari K. Gaussian-4 theory using reduced order perturbation theory. *J Chem Phys* 2007;127:124105-13. DOI
45. Frisch MJ, Trucks GW, Schlegel HB, et al. Gaussian 16. Wallingford CT; 2016. Available from: <https://gaussian.com/> [Last accessed on 4 May 2023].
46. Betz J, Brinkmann J, Nölle R, et al. Cross talk between transition metal cathode and Li metal anode: unraveling its influence on the deposition/dissolution behavior and morphology of lithium. *Adv Energy Mater* 2019;9:1900574. DOI
47. Kühn SP, Edström K, Winter M, Cekic-laskovic I. Face to face at the cathode electrolyte interphase: from interface features to interphase formation and dynamics. *Adv Mater Interfaces* 2022;9:2102078. DOI
48. Bieker G, Winter M, Bieker P. Electrochemical *in situ* investigations of SEI and dendrite formation on the lithium metal anode. *Phys Chem Chem Phys* 2015;17:8670-9. DOI PubMed
49. Wood KN, Noked M, Dasgupta NP. Lithium metal anodes: toward an improved understanding of coupled morphological, electrochemical, and mechanical behavior. *ACS Energy Lett* 2017;2:664-72. DOI
50. Jung R, Metzger M, Haering D, et al. Consumption of fluoroethylene carbonate (FEC) on Si-C composite electrodes for Li-ion batteries. *J Electrochem Soc* 2016;163:A1705-16. DOI
51. Stolz L, Gaberšček M, Winter M, Kasnatscheew J. Different efforts but similar insights in battery R&D: electrochemical impedance spectroscopy vs galvanostatic (constant current) technique. *Chem Mater* 2022;34:10272-8. DOI
52. Hobold GM, Lopez J, Guo R, et al. Moving beyond 99.9% Coulombic efficiency for lithium anodes in liquid electrolytes. *Nat Energy* 2021;6:951-60. DOI
53. Ota H, Sakata Y, Otake Y, Shima K, Ue M, Yamaki J. Structural and functional analysis of surface film on Li anode in vinylene carbonate-containing electrolyte. *J Electrochem Soc* 2004;151:A1778. DOI
54. Nie M, Demeaux J, Young BT, et al. Effect of vinylene carbonate and fluoroethylene carbonate on SEI formation on graphitic anodes in Li-ion batteries. *J Electrochem Soc* 2015;162:A7008-14. DOI
55. Grugeon S, Jankowski P, Cailieu D, et al. Towards a better understanding of vinylene carbonate derived SEI-layers by synthesis of reduction compounds. *J Power Sources* 2019;427:77-84. DOI
56. Freunberger SA, Chen Y, Peng Z, et al. Reactions in the rechargeable lithium-O₂ battery with alkyl carbonate electrolytes. *J Am Chem Soc* 2011;133:8040-7. DOI
57. Bryantsev VS, Blanco M. Computational study of the mechanisms of superoxide-induced decomposition of organic carbonate-based electrolytes. *J Phys Chem Lett* 2011;2:379-83. DOI
58. Sinha A, Thomson M. The chemical structures of opposed flow diffusion flames of C₃ oxygenated hydrocarbons (isopropanol, dimethoxy methane, and dimethyl carbonate) and their mixtures. *Combust Flame* 2004;136:548-56. DOI
59. Atkinson R. Atmospheric reactions of alkoxy and β-hydroxyalkoxy radicals. *Int J Chem Kinet* 1997;29:99-111. DOI